Nuclear inelastic scattering studies of lattice dynamics in magnetite with a first- and second-order Verwey transition

Tomasz Kołodziej,[1] Andrzej Kozłowski,[1] Przemysław Piekarz,[2] Wojciech Tabiś,[1] Zbigniew Kąkol,[1] Marcin Zając,[3]
Zbigniew Tarnawski,[1] Jürgen M. Honig,[4] Andrzej M. Oleś,[5] and Krzysztof Parlinski[2]

[1]*Faculty of Physics and Applied Computer Science, AGH-University of Science and Technology,
Aleja Mickiewicza 30, PL-30059 Kraków, Poland*
[2]*Institute of Nuclear Physics, Polish Academy of Sciences, Radzikowskiego 152, PL-31342 Kraków, Poland*
[3]*ESRF, 6 rue Jules Horowitz, F-38043 Grenoble, France*
[4]*Department of Chemistry, Purdue University, West Lafayette, Indiana 47907-2084, USA*
[5]*M. Smoluchowski Institute of Physics, Jagellonian University, Reymonta 4, PL-30059 Kraków, Poland*

Nuclear inelastic-scattering studies were performed to infer temperature evolution of iron atom dynamics in magnetite samples exhibiting Verwey transition of first- and second-order (type-I and type-II materials). The possible difference in this evolution could rationalize the distinct properties of these classes of materials observed in heat capacity and diffuse scattering below the Verwey transition temperature T_V and could explain the change in transition order triggered by a minute (below 0.3%) altering of the iron sublattice. Although we have found the apparent stiffening of the phonon iron spectrum in the low-temperature phase, at the same time, we have shown that these spectra are rather similar for type-I and type-II materials, rendering the lattice vibration-based explanation of the distinct behavior of heat capacities very improbable. The calculation of phonon spectra, aimed at tracing the origin of various features in the phonon density of states (DOS), has shown that the local Coulomb interaction U may have a large effect on phonon DOS. However, the change in the U parameter cannot explain the difference in heat-capacity results for both classes of materials. Thus, an additional factor that differentiates these materials and possibly is responsible for the discontinuous character of the Verwey transition in stoichiometric magnetite still must be found.

I. INTRODUCTION

Magnetite is well known for its extensive use in traditional recording media but also for its role in the emerging field of spin electronic applications.[1] It is also the most abundant natural magnetic material that can store the memory of the past in the magnetic order formed while cooling down from a liquid state. Apart from its wide application, this is the fascinating material where, in a structure made of only two elements, the abundance of phenomena, representative for almost all the condensed matter, is astonishing and is still to be explained. One of those phenomena is the Verwey transition, the first-order phase transformation at $T_V = 122$ K where many physical properties exhibit spectacular anomalies. The other is magnetite sensitivity to a slight disturbance in the lattice by doping or nonstoichiometry: Already, 0.3% of defects cause the sudden change in transition character. In this paper, the change in transition order is discussed in correlation with the lattice dynamics studied by the nuclear inelastic scattering (NIS) of x rays.

The Verwey transition is best recognized by a 2-order-of-magnitude resistivity jump at T_V [Fig. 1(a), based on Ref. 2] and a huge peak in heat capacity,[3] although anomalies are observed practically in all physical characteristics, including the symmetry that changes from high-temperature cubic to the monoclinic at $T < T_V$.[4] The fact that the electrical transition is simultaneous with the structural one suggests that the coupling between electronic states and crystal lattices may play an important role in the mechanism leading to the transition. Indeed, the substitution of 43% of normal ^{16}O by the heavier ^{18}O resulted in a considerable increase in the Verwey

temperature by approximately 5 K.[5] And the neutron studies of diffuse scattering[6–8] suggested that the lattice prepares for the transition already 80 K above T_V. Recent theoretical analysis[9] has confirmed the crucial role of electron-phonon and electron-electron correlations in the mechanism of the transition pointing to, at least, three phonon modes that are at the origin of the observed low-temperature phenomena: (i) a X_3 phonon optic mode (at 17 meV), mainly composed of iron vibrations, has been shown to considerably lower the electronic energy and to open the insulating gap, ultimately leading to the change in structure, i.e., the transition; (ii) a zone-center optic mode of T_{2g} symmetry (24–33 meV), related to the c_{44} elastic constant, already behaves critically 80 K above T_V (Ref. 10) as also suggested by neutron studies;[8] (iii) the critical behavior of the third important mode Δ_5 (8 meV) is observed just a few Kelvin above T_V,[6] which may be linked to the second crucial finding of recent years[11]: Charge (and orbital) orders also start ∼8 K above T_V. Such charge-orbital ordering exists in magnetite due to strong local Coulomb interaction U between the $3d$ electrons in iron atoms as demonstrated by the *ab initio* studies.[12–14] All those facts clearly state that electron-electron and electron-phonon interactions are the key points in the understanding of the Verwey transition.

Electron-electron and electron-phonon interactions can be finely tuned by doping or nonstoichiometry. If nonstoichiometry parameter 3δ in $Fe_{3(1−\delta)}O_4$ [Fig. 1(a)] or doping x in $Fe_{3x}(Zn,Ti)_xO_4$ exceeds the universal value of $3\delta = x = 0.012$, the original first-order Verwey transition (type-I samples) turns to the continuous one (type-II) that disappears altogether for $3\delta = x > 0.04$.[2] With doping and nonstoichiometry, the transition temperature lowers linearly, but the T_V vs
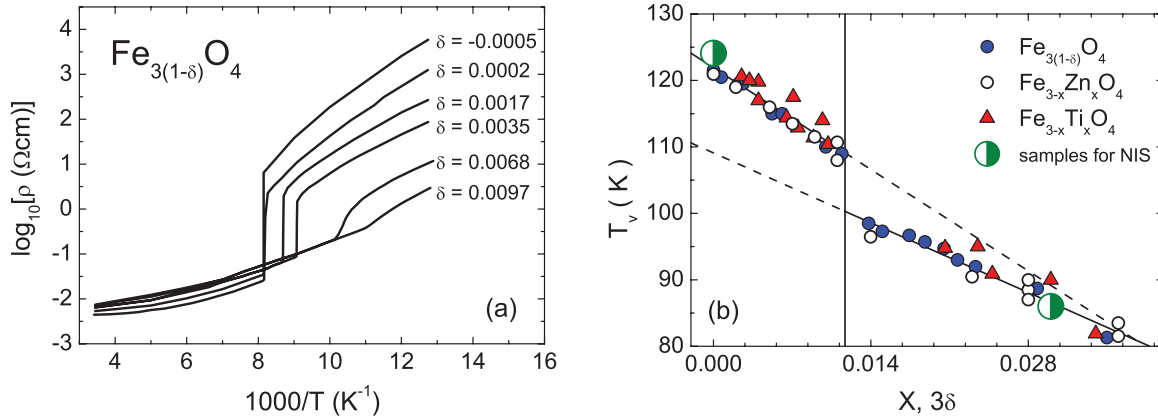
FIG. 1. (Color online) Resistivity vs inverse temperature for magnetite $Fe_{3(1-\delta)}O_4$ with different stoichiometry parameters (based on Ref. 2) (a) and the universal T_V vs $3\delta = x$ relation (based on Ref. 2 with subsequent results added). Note the change in transition order manifested by the transition spreading (a) and the corresponding two slopes in (b). The composition of the samples used for the present studies are marked by large bullets.

$x = 3\delta$ relation [see Fig. 1(b)] has two different slopes, clearly delimiting both regions. Also, some universality is observed here since the scaling $x = 3\delta$ occurs in cases of Zn and Ti doping and nonstoichiometry parameter 3δ despite the fact that Zn atoms enter tetrahedral lattice positions, titanium octahedral, while vacancies also are formed on octahedral sites. The influence of other elements on the transition order is similar, although the universal scaling no longer is satisfied.[15] No explanation for the disturbing effect of extraneous elements on the Verwey transition was suggested so far.

Magnetite properties at $T > T_V$ do not distinguish type-I and type-II materials. In our elastic constant studies,[10] we have found that the c_{44} mode for stoichiometric and Zn-doped magnetite shows increasing softening already starting at high temperatures, irrespective of transition order. Also, whatever the transition order, c_{44} for all measured samples are very well fitted by the formula $c_{44} = c_{44}^0 \frac{T - T_C}{T - \theta}$, based on Landau theory of continuous phase transitions with the same parameters: $\theta = 56$ and $T_C = 66$ K. Thus, one may expect that not only the system prepares for some low-temperature transition in the same manner, irrespective of its order (this is represented here by θ), but also the coupling to the elastic degrees of freedom is the same (represented by T_C). The critical behavior of c_{44} above T_V has been confirmed also in the extended Landau theory of the first-order phase transition with two primary-order parameters.[16] Apparently, high-temperature properties [such as elastic constants but also heat capacity at $T > T_V$ (Ref. 17) and the structure[18]] are not sensitive to doping and do not differentiate between first- and second-order-type materials. As observed from the high-temperature side, a continuous phase transformation already started to develop for all materials at high temperatures but, for type-I materials, was terminated by some other effects just above T_V ultimately triggering the discontinuous Verwey transition.

In contrast, many low-temperature properties are different for magnetite of first and second order. In neutron studies of the diffuse scattering,[8] it was found that, while this effect diminishes abruptly at T_V for first-order samples [see Fig. 2(a)], the intensity for second-order nonstoichiometric magnetite gradually increases down to the lowest temperatures, showing

only a change in slope at T_V. The differences between both classes are even more apparent from the inspection of the temperature dependence of the heat capacity [Fig. 2(b)]: The drop in the heat-capacity background below T_V for the first-order samples is seen, while there is a continuous evolution of this background for second-order materials.[17] The temperature dependence of the Debye temperature θ_D, extracted from heat-capacity data, accentuates this finding. All of these facts point to the lattice getting more rigid below T_V for the first-order magnetite, with no particular change for type-II materials. Thus, the general conclusion is that the transition order may be linked to different lattice dynamics and/or different electron-phonon couplings observed by the lattice dynamics.

The lattice stiffening below T_V was partly confirmed[19] for a stoichiometric single-crystalline magnetite film by means of the NIS. Based on the experimental results and their comparison with the calculated phonon density of states (DOS), the conclusion was drawn that the octahedral iron vibration spectrum slightly shifts discontinuously toward higher energies while the temperature falls below T_V. Also, some results of optic papers of phonon modes support this conjecture (although for higher-energy modes),[20,21] but no clear change in the phonon dispersion relation at low energies at T_V was found in the inelastic neutron scattering in a magnetite single crystal.[22] In any case, the problem, if the lattice dynamics is altered at T_V for type-I materials and remains virtually intact for magnetite with the second-order Verwey transition and if this possible difference in phonon spectrum is linked to the change in transition order, is never directly addressed; the present experiment is meant to fill this gap. Phonon densities of states [DOS $\equiv g(E)$] for iron atoms were observed directly by the NIS on the ID18 beamline in the European Synchrotron Radiation Facility (ESRF) for two samples, with discontinuous and with continuous transitions. Since lattice dynamics alone should not be altered by a minute 1% substitution of different atoms, we expected the change in electron-lattice coupling that could trigger the observed phenomena. Phonon DOS also were calculated to see their dependence on electron correlation and to identify the particular features in measured DOS. The net
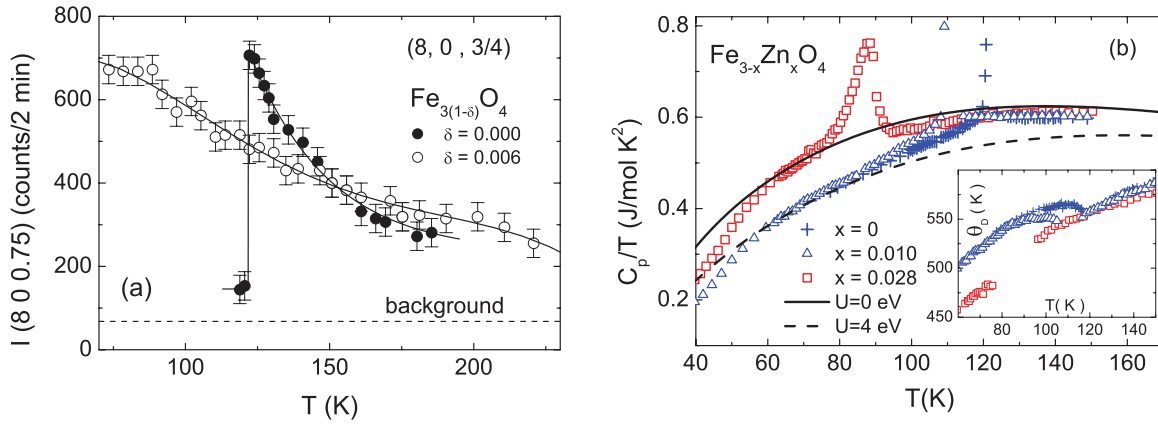
FIG. 2. (Color online) Experimental characteristics that differentiate between the Verwey transition of first and second orders. (a) Temperature dependence of the diffuse scattering at $(8\ 0\ \frac{3}{4})$ for $\delta = 0$ (type-I) and $\delta = 0.006$ (type -II) materials (after Ref. 8). (b) The temperature dependence of heat capacity in $Fe_{3-x}Zn_xO_4$. The baseline for $x = 0.028$ (second-order transition) at $T < T_V$ is larger than for first-order samples as better seen in the T dependence of Debye θ_D (the inset; the peak is removed for clarity). For $T > T_V$, the backgrounds are identical (after Ref. 17). Solid and dashed lines are heat-capacity baselines calculated from theoretical curves (see the text). Note that constant pressure heat capacity C_p is measured, while constant volume C_V is calculated.

result of our studies is that, although there is some stiffening of the lattice below T_V, this change is very similar for type-I and type-II materials. Thus, some other factor, not a distinct lattice dynamics, is responsible for a drastic difference in heat capacity and the diffuse scattering in both classes of materials.

The paper is organized as follows. The experimental and theoretical methods are presented in Sec. II, while the results, i.e., the experimental data and the density of states obtained by the *ab initio* calculations are given in Sec. III. Our results are discussed in Sec. IV. In particular, after the general comments in Sec. IV A, in Sec. IV B heat capacity for the stoichiometric and doped magnetite is calculated from the phonon DOS and is compared with the experimental data. In Sec. IV C, the temperature change in experimental DOS is analyzed, and we compare our results with the phonon DOS obtained previously for the thin film. Finally, the mechanisms of the first- and second-order Verwey transition are discussed in Sec. IV D. Here, the main conclusions also are presented.

II. EXPERIMENTAL AND THEORETICAL METHODS

Since very small doping or nonstoichiometry levels greatly affect the Verwey transition, it is obvious that proper sample preparation procedures are crucial for the reliability of the experimental results. The measurements were performed on single-crystalline samples grown at Purdue University by the skull melter crucibleless technique.[23] This technique allows for the control of oxygen partial pressure during growth, thereby ensuring that the melt remains within the stability range of the material. After preparation, the crystals are subjected to subsolidus annealing under CO/CO_2 gas mixtures to establish the appropriate metal/oxygen ratio.[24] Two single-crystalline samples, with a natural abundance of the ^{57}Fe isotope, were measured: stoichiometric magnetite and $Fe_{3-x}Zn_xO_4$ with $x = 0.03$, displaying Verwey transition of second-order [see Fig. 1(b)].

The NIS measurements[25] were performed at the nuclear resonance beamline ID18 (Ref. 26) of the ESRF during the

16 bunch mode of synchrotron operation. A high-intensity synchrotron x-ray beam was monochromatized for the resonant transition in the nuclei of the ^{57}Fe with energy of 14.412 keV using a high-resolution optics. The energy of the incident radiation is varied in the vicinity of the nuclear transition by scanning the angle of the high-resolution monochromator crystals. Such a procedure allows either to annihilate (negative E) or to excite phonons (positive E) in the sample while incoherently exciting iron nuclear states. After deexcitation, the delayed quanta are collected by an avalanche photodiode in two channels. The first one, located close to the sample to cover a large solid angle, measures the incoherent-scattering signal providing information about the probability of inelastic nuclear absorption. The second one, located far away from the sample, monitors coherent nuclear forward scattering constituting the instrumental function of the high-resolution monochromator;[27] for this experiment, the resolution was equal to 0.85 meV.

Samples [of a thickness of <0.1 mm, with the exposed (001) plane] were glued to thin sapphire plates (approximately 0.16 mm) and were placed on specially made sample holders that allowed one to control sample inclination vs incoming radiation; the best results, i.e., strongest NIS signal and instrumental function, were obtained at an $\sim 45°$ inclination. For such geometry, the beam focal spot on the sample was about $10 \times 10\ \mu m^2$. The sample temperature was monitored both by the system thermometer placed on the cold finger and by the Pt thin-film thermometer glued directly to the sample.

NIS measurements were performed in the range up to 100 meV from the resonance energy with a 0.2-meV grid and at two temperatures below and two above the Verwey transition temperature. The average count rate in the intensity maximum of the inelastic part was around 4 per second, and few dozens of scans, each lasting approximately 40 min, were required to obtain reasonable statistics at 50 and 150 K. Due to time constraints, for middle-temperature measurements (at 65 and 135 K), several shorter scans were performed. At most temperatures, the coherent nuclear forward-scattering signal

(the so-called time spectrum) was collected to additionally control the occurrence of the transition. Data processing to extract partial phonon DOS from inelastic-scattering data was performed following the procedure described in Ref. 28; we estimate that, due to subtraction difficulties of the elastic central part, $g(E)$ are reliable in energy range $E > 3.5$ meV.

We performed the *ab initio* calculations of phonon DOS to enable the rationalization of measured spectra. The electronic and crystal structures of Fe_3O_4 were optimized within the density functional theory, using the projector augmented-wave method[29,30] implemented in the VASP package.[31] The exchange-correlation energy has been optimized within the generalized gradient approximation.[32]

The local interactions between *3d* electrons in iron atoms are described using the degenerate Hubbard Hamiltonian by the Coulomb element U and Hund's exchange J within the local-density approximation $+ U$ method.[33] In the present calculations, we have used the same values of parameters as in the previous papers:[9] $U = 4$ and $J = 0.8$ eV. For comparison, in order to investigate the effect of local interactions on phonons, we also have included the results obtained for $U = J = 0$. All calculations were performed using the crystallographic face-centered-cubic supercell containing 56 atoms with the periodic boundary conditions. The Brillouin zone integration was carried out on the $6 \times 6 \times 6$ wave-vector Monkhorst-Pack mesh.[34] The energy cutoff for the plane-wave expansion was set at 520 eV.

The phonon frequencies were determined by the direct method,[35] implemented in the PHONON program.[36] The Hellmann-Feynman (H-F) forces were computed for positive and negative atomic displacements with the amplitude of 0.02 Å. All displaced configurations generate 1008 components of the H-F forces. The so-called cumulant force constants were fitted to the H-F forces by the singular value decomposition method.[36,37] According to the direct method, the exact phonon frequencies were obtained at high-symmetry points Γ and X. The force constants diminished by more than 2 orders of magnitude within the supercell, and this allowed us to derive reasonable phonon frequencies at all wave vectors. The force constants were used to construct the dynamical matrix, to diagonalize it, and to find the phonon frequencies.

III. RESULTS

Time spectra of the nuclear forward scattering were measured to initially observe the difference in sample properties below and above T_V and to see the distinct behavior for each sample at the same temperature. This last issue is addressed in Fig. 3, where the comparison between samples at 50 and 150 K is presented. Note that the quantum beats pattern is almost identical at low T, and similar, although with different amplitude, at 150 K. This similarity between samples is not so well reflected in Mössbauer incoherent spectra, measured for these particular samples.[38]

The temperature evolution of DOS curves, for each sample, is presented in Figs. 4 and 5; full DOS curves are shown only for the highest and lowest temperatures measured, while all curves are shown using $g(E)/E^2$ vs E coordinates, to account for the possible quadratic energy dependence of phonon DOS in the low-energy range. In the inset of Fig. 4(a), the features, present in both samples, are marked. Note a pronounced difference between the data above and below T_V in the energy region $E < 15$ meV as well as a clear temperature change in the second peak at 24 meV. The other features of the spectra are the temperature shift of the first peak at 18.5 meV to lower energies on heating and the change of the small, but reproducible, anomaly at 19.8 meV. Although these features are shown here only for $x = 0$, they also exist and behave similarly for the $x = 0.03$ sample.

The comparison of phonon DOS for two samples at temperatures below and above T_V are shown in Figs. 6 and 7; in both figures, panels (a) present the full energy range, and panels (b) present the range for $E < 30$ meV and in the $g(E) \sim E^2$ parametrization. The insets in Figs. 6(a) and 7(a) show the comparison between samples in the low-energy parts of the spectra. It is clear that the dominant features of Fe DOS are almost identical for both samples. The secondary structures slightly differ, but it does not change the overall outcome that the similar lattice dynamics of both samples cannot rationalize the difference between first- and second-order materials. Figures 5 and 6 confirm the results obtained previously[19] that these DOS are different below and above the Verwey transition.
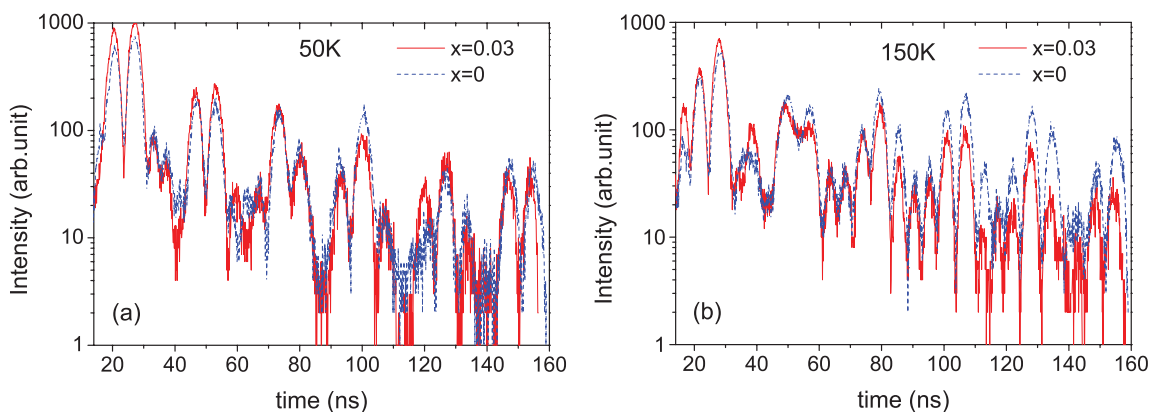
FIG. 3. (Color online) The comparison of time spectra from different samples at (a) 50 K and (b) 150 K, proving the similarity of the hyperfine splitting (to a higher extent at $T < T_V$).
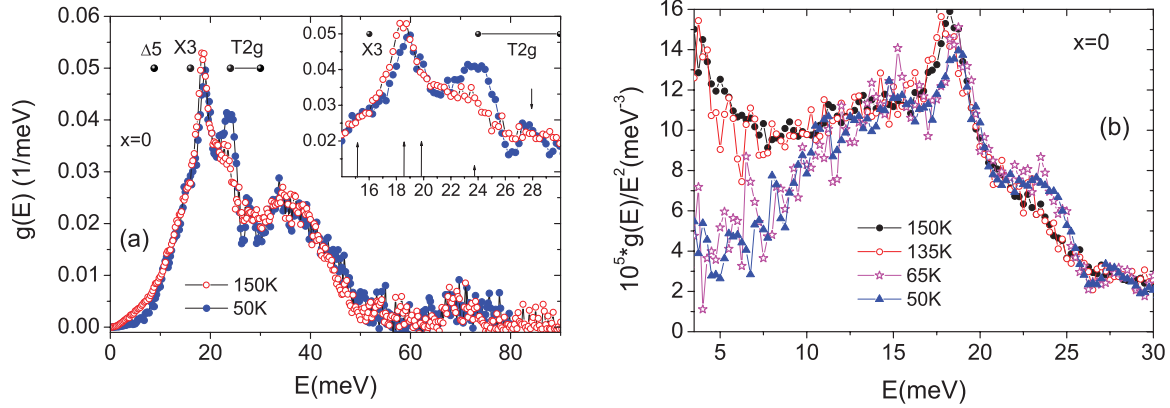
FIG. 4. (Color online) Experimental Fe DOS for stoichiometric magnetite [here and in Figs. 5–7, $g(E)$ is per the Fe atom, unlike in Figs. 8 and 9, where the DOS were normalized to the formula unit]. In the full spectra (a) only the data for temperatures at 50 K (below T_V) and 150 K (above T_V) are shown, while the DOS divided by E^2 to check the quadratic $g(E)$ relation are plotted in panel (b) for all measured temperatures. In the inset of panel (a), a lower-energy part is presented, and the characteristic structures as well as phonon modes, mentioned in Ref. 9, are marked.

Phonon DOS, calculated for $U = 4$ and $U = 0$ eV, are presented in Fig. 8. For $U = 4$ eV, the phonon spectra are shifted to higher energies due to a stronger localization of electrons and a weaker screening of interatomic forces.[9] The partial octahedral and tetrahedral iron spectra are shown off scale in comparison to total and oxygen vibrations.

In Fig. 9, the comparison of calculated DOS with the experimental data for $x = 0$, representing dominant features for both samples, is shown (since the spectra for both samples are very similar, the comparison for $x = 0.03$ is not presented). Here, the tetrahedral Fe DOS is superimposed on the total (iron) one, and the cases with $U = 4$ and $U = 0$ eV are presented separately. The experimental data seem to be better reproduced by theoretical DOS if the electron correlation term is included ($U = 4$ eV). In particular, the position and the width of the main band around 18 meV agrees much better with the experiment. Also, the agreement for the second band between 22 and 27 meV is improved significantly compared to calculations with $U = 0$, which gives much weaker intensity in this energy range.

IV. DISCUSSION AND SUMMARY

A. General considerations

The main idea, after the NIS measurements, was to find the experimental confirmation of the distinct lattice dynamics at low T in magnetite of first and second orders; such a difference could rationalize many experimental results, in particular, the drastic difference between low-T heat capacity and diffuse scattering of those materials. Already, a rough inspection of the presented data (Figs. 6 and 7) shows that phonon density of states for both samples are nearly the same and, as forthcoming analysis implies, cannot explain the differences in heat capacity. In the experimental data presented in Figs. 4 and 5, in particular, in the inset of Fig. 4, the characteristic structures, specific for both samples, are marked. These are as follows:

(1) The increase in DOS in the vicinity of 7 meV at $T > T_V$ in comparison to the low-T spectrum.

(2) The ensuing shift in the center of gravity of the 16–26 meV part of the spectrum to lower energies on heating.
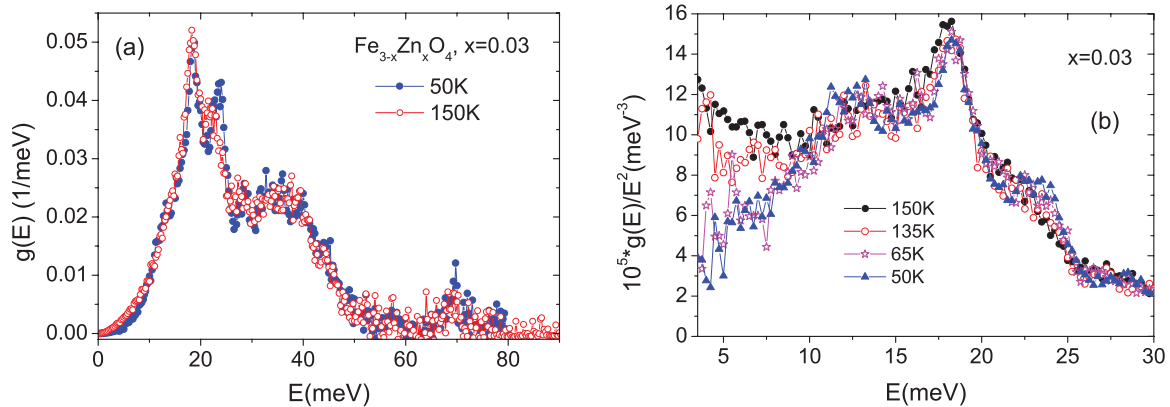
FIG. 5. (Color online) Experimental Fe DOS for the Zn-doped sample. Note the difference between low- and high-temperature spectra, mainly below $E = 15$ meV and around the second peak at 22 meV, the feature present in both samples.
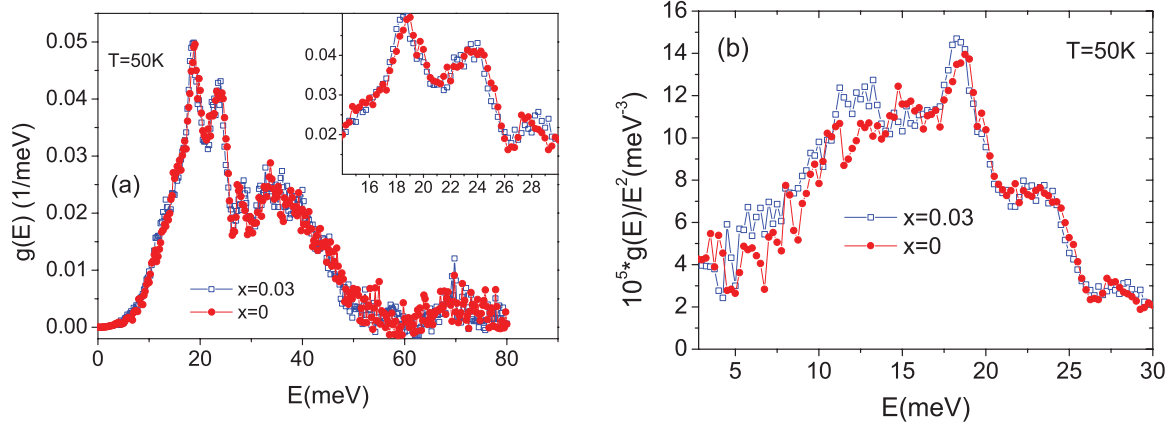
FIG. 6. (Color online) Comparison of experimental partial DOS for both samples at 50 K in (a) full and (b) limited energy ranges. In the inset of panel (a), a lower-energy part is presented using a better resolution.

(3) Three peaks at $E = 18.5$, 19.8, and 22–25 meV that are subject to this shift.

(4) The peak at 28 meV that does not seem to be temperature/crystal structure dependent.

Some of these features will be addressed below under the appropriate headings.

We have performed *ab initio* phonon calculations to support experimental analysis, in particular, to understand the origin of the above-mentioned structures in experimental DOS and their possible sensitivity to external factors (as, e.g., doping). These factors were mimicked by a varying strength in U and J: We have performed calculations both for $U = 4$ and for $J = 0.8$ eV, and $U = J = 0$ as in Ref. 9.

From Fig. 8, it is apparent that the low-energy part of the whole spectrum is due to iron vibrations. So, our experimentally obtained iron DOS roughly represents the whole magnetite lattice vibration below $E = 20$ meV. There is a rich low-energy (below 20-meV) structure of iron transverse acoustic lattice vibrations, mainly dominated by octahedral sites with only limited tetrahedral iron participation, except in the case of $U = 0$ where tetrahedral iron vibrations are of a slightly higher intensity (see also Fig. 9, where the comparison of calculated and measured DOS is shown). The peaks between 30 and 40 meV are due to dynamics in both sites with their almost equal participation. Oxygen atoms remain inactive below $E = 30$ meV in the case of Coulomb $U = 0$

and below 40 meV when strong correlations are taken into account, the fact best seen in Fig. 8. At higher energies, the spectrum is dominated mainly by oxygen vibrations that couple to tetrahedral Fe atoms at ∼70 meV.

As in the previous studies,[19] our calculations were performed assuming the cubic low-temperature structure. The calculations for the real Cc low-T structure were not attempted due to both their complications but also due to our belief that this monoclinicity is small enough to roughly represent lattice vibrations also below T_V. In fact, type-I and type-II materials undergo similar lattice symmetry changes, rendering the clear difference between them to some other than structural reason. In particular, the main large features of experimental Fe DOS, the peaks at 18.5 and at 35 meV, are similar at both temperature regimes and in both samples, which makes our assumption of a similar vibration spectrum for both crystal structures highly probable.

In the rest of the paper, some issues mentioned above are discussed further.

B. Heat Capacity

As already mentioned above, our main task was to check if different lattice vibrations for type-I and type-II magnetite could account for heat-capacity results.
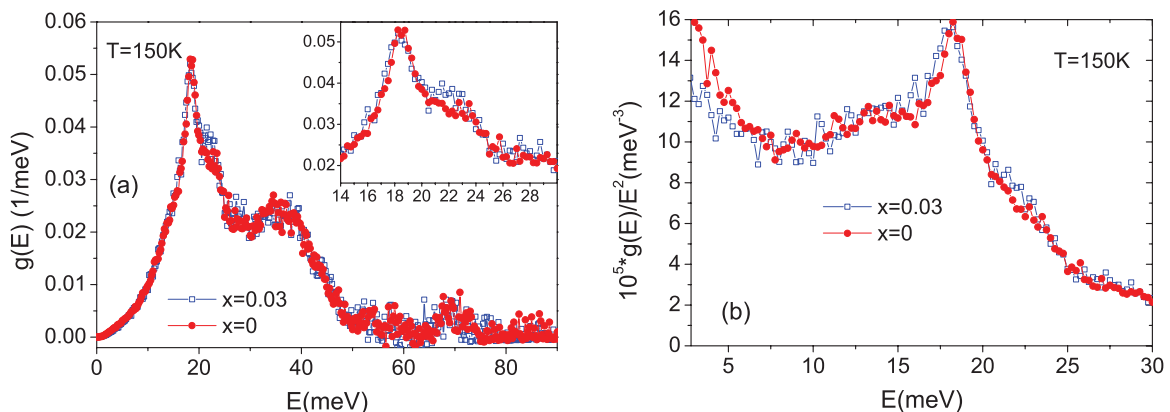
FIG. 7. (Color online) Same as in Fig. 6 but at 150 K. Note that $g(E)$ for both samples and both temperatures are nearly identical.
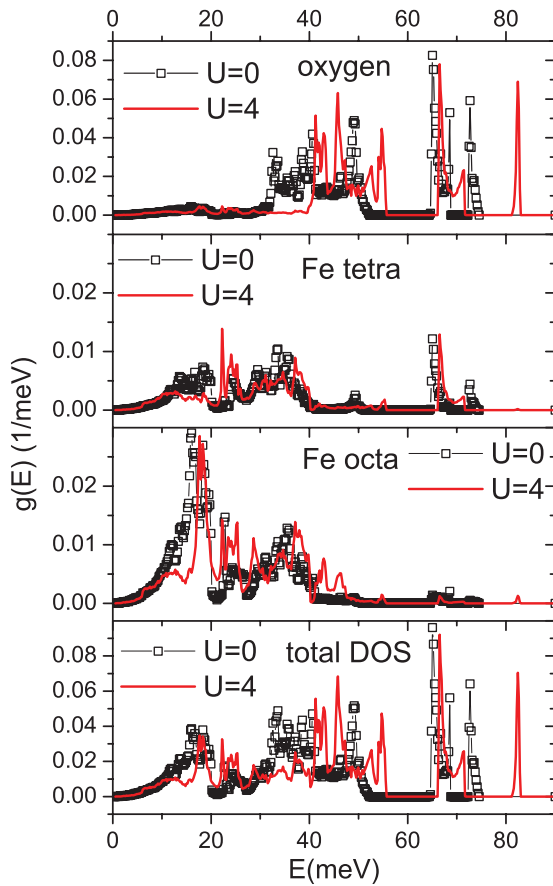
FIG. 8. (Color online) Calculated phonon DOS for the magnetite cubic phase for the electron-electron correlation parameter $U = 0$ eV (squares) and $U = 4$ eV (line, red online). Note that Fe DOS scales are expanded in comparison with total and oxygen DOS.

The temperature dependence of heat capacity, calculated from the theoretical DOS and presented in Fig. 2, is compared with experimental results for stoichiometric magnetite and Zn-doped ferrite. Apparently, the DOS for $U = 4$ eV very roughly describes the experiment for stoichiometric magnetite below T_V, already falling below the experimental result at about $T > 80$ K. On the other hand, both the experimental results

for the type-II sample as well as the data for the type-I sample, but at $T > T_V$, are reasonably well approximated by the DOS obtained with $U = 0$. It might suggest that lattice dynamics for samples with the continuous Verwey transition and those with the transition of the first order, but at $T > T_V$, results from the electronic structure with $U = 0$, while a considerably higher correlation sets in at T just below T_V, resulting in an abrupt first-order transition and the diminished lattice vibration contribution. However, the similarity in the vibration spectra for type-I and type-II samples, proved by our experiment, strongly contradicts this conjecture. Thus, the experimental rather than the theoretical Fe vibration spectrum should be used for heat-capacity calculation.

The heat capacity obtained based on experimental Fe DOS and calculated oxygen DOS is presented in Fig. 10. Although we do not expect pronounced differences in the oxygen vibration spectrum for both samples, we have, nevertheless, calculated the heat-capacity curve, using different theoretical oxygen DOS in both T ranges: oxygen DOS calculated for $U = 0$ and that for $U = 4$ eV were used for $T > T_V$ and $T < T_V$, respectively. Clearly, the apparent excess of experimental heat capacity at $T < T_V$ for the doped sample with continuous Verwey transition cannot be explained by the different lattice vibrations, even if different oxygen DOS are used.

C. Temperature dependence of the DOS

Figures 4 and 5 show the clear difference between lattice vibrations at $T > T_V$ and $T < T_V$, similar for samples exhibiting Verwey transition of both kinds (Figs. 6 and 7). Upon heating across the Verwey transition, the phonon density of states increases at low energies, below 10 meV, which is slightly stronger for the stoichiometric samples than for the Zn-containing one [see Fig. 7]. The peak at 18.5 meV, possibly the X_3 phonon mode, gains intensity, whereas, the structure at the energy range of 22–26 meV, probably linked to T_{2g} optic modes, loses intensity and so, is similar to the small peak at 19.8 meV [see the inset in Fig. 4(a)]. This change is less apparent in the case of the Zn-doped sample [compare the insets of Figs. 6(a) and 7(a)]; actually, the peak at 19.8 meV is practically temperature independent in this case.
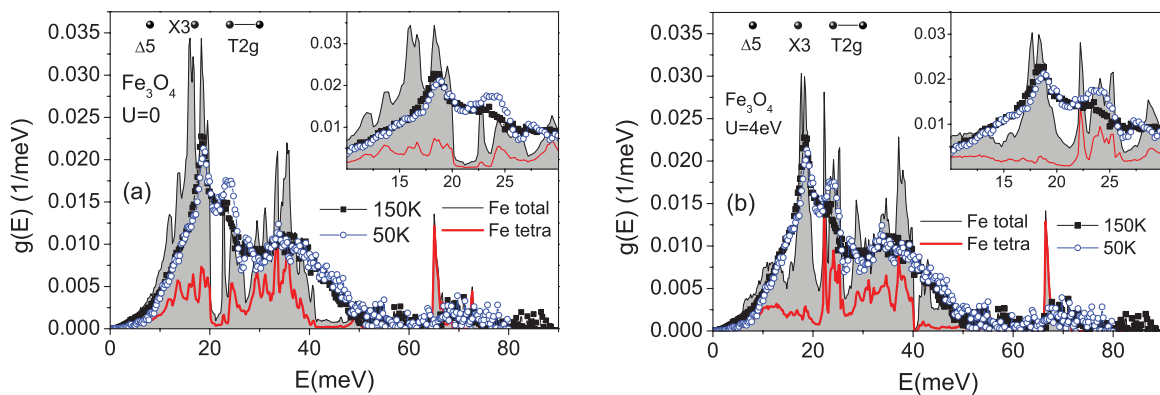
FIG. 9. (Color online) Comparison of measured DOS, for stoichiometric magnetite and at $T = 50$ and 150 K (points + lines), with calculated total DOS for iron (lines) for $U = 0$ [panel (a)] and $U = 4$ eV [panel (b)]; in each case, the tetrahedral component is presented separately. In the insets, the important low-energy region is shown.
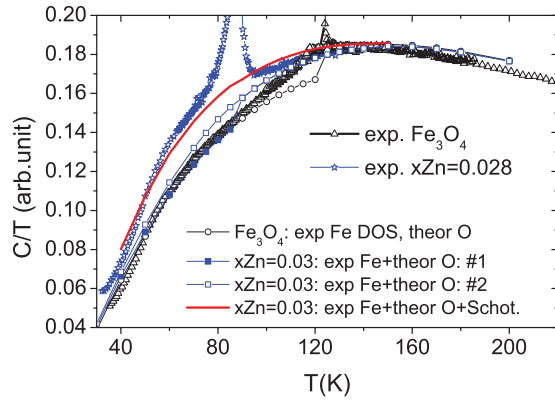
FIG. 10. (Color online) Experimental heat capacity (C_p) curves for $x_{Zn} = 0.028$ (stars, blue online)[17] and stoichiometric magnetite sample (triangles) compared to calculated curves (C_V). For iron vibration, the measured DOS were used. For the stoichiometric sample (hollow black bullets), oxygen vibrations were described by calculated DOS with $U = 4$ eV at $T < T_V$ and with $U = 0$ for $T > T_V$. For the Zn-doped sample, either the same procedure was applied (#1, bulk blue squares), or $U = 0$ oxygen DOS was used (#2, open blue squares) Note that the low-temperature upturn for type-II samples is not reproduced in any case. Finally, the Schottky-like two-level system model with an energy separation of ~170 K and equal degeneracies was used in addition to experimental Fe DOS for $x_{Zn} = 0.03$ and oxygen vibrations for $U = 0$ (red line). Note also that the large heat-capacity peak for stoichiometric magnetite was only marked.

To accentuate the behavior of the low-energy part of the spectrum, the data were rescaled to $g(E)^*E^2$ vs E coordinates (Fig. 11). Here, while for the pure sample where a loss of weight is seen around 24 meV, it seems that the weight is transferred to 21 meV for the Zn-containing sample. Interestingly, such a downshift also is found in a 500-nm monocrystalline thin film, measured previously[19] and depicted in Fig. 11. The comparison of the present measurements for the stoichiometric sample with those for the thin film is also presented in Fig. 12 (note that, while our present measurements were performed on samples prepared from natural iron, the enriched iron was used previously). Although the data are very similar and all the details are reproduced in the results of our experiment, the present spectrum is shifted into higher energies (in a similar way as in Ref. 39) possibly due to substrate strain in the thin film. Thus, the downshift in the 22–26-meV part of the spectrum in the Zn-doped sample also may be ascribed to strain caused by dopants.

As already mentioned above and as inferred from Fig. 9, the spectrum for $E < 22$ meV is dominated by octahedral iron vibration. On the contrary, the second peak at $E = 24$ meV may contain quite a large tetrahedral component (see Fig. 9, the $U = 4$-eV case), and the much more pronounced changes in temperature of this peak, suggesting its different origin, might support this conjecture. On the other hand, no other data exist that could confirm the change in the tetrahedral vibration spectrum at T_V, and the integrated DOS up to ~25 meV (the rough termination point of the second peak) at 50 and 150 K are almost identical [within 3% of the total integrated $g(E)$ for this energy] for each sample. It suggested that both
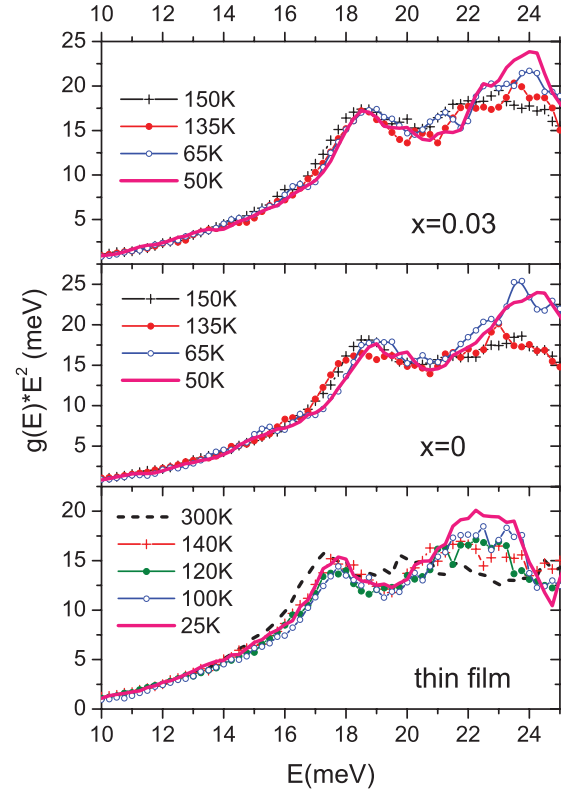
FIG. 11. (Color online) Measured DOS for both samples as well as the results from Ref. 19 in $g(E)^*E^2$ for increasing the energy E representation to amplify the changes in the second peak. Unlike in previous results, this peak also seems to be related to the Verwey transition.

features, the low-energy gap for $E < 10$ meV and the second peak, were correlated, i.e., some low-energy vibrations of octahedral iron atoms, active at high temperatures, increased their energy once the temperature crossed T_V, which resulted in the spectrum center of the gravity shift to higher energies in the low-temperature phase. In other words, the octahedral
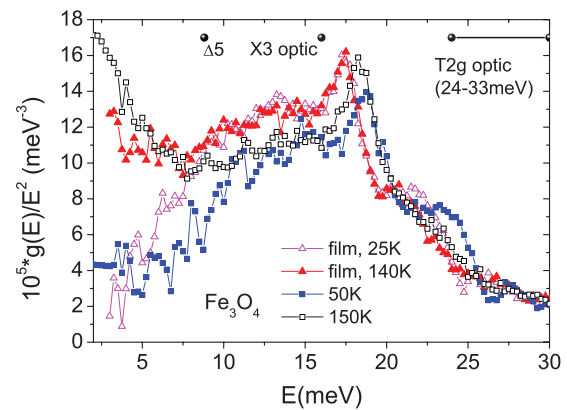
FIG. 12. (Color online) Fe DOS for the stoichiometric magnetite bulk sample as well as for the stoichiometric thin film[19] at low and high temperatures and in g/E^2 vs E coordinates. The gap starting below $E = 10$ meV is apparent for both samples, although the spectrum for the bulk crystal is shifted to higher energies. Bullets show Δ_5 and X_3 phonon modes as calculated in Ref. 9.

iron lattice becomes more rigid at low temperatures, as suggested a long time ago, but this process is very similar for samples undergoing the Verwey transition of first and second orders.

The change in the phonon DOS at low energies of $E < 10$ meV can be related to the recently observed[40] strong anharmonicity in the lowest transverse acoustic branches. We remark that anomalously large phonon widths have been found above the Verwey transition by the inelastic x-ray scattering measurements. This anharmonic effect already was observed at high temperatures ($T \sim 300$ K) and became larger with lowering the temperature toward T_V, indicating strong electron-phonon interaction driving the Verwey transition. This electron-phonon coupling is especially strong for the octahedral iron sites where the charge-orbital ordering takes place. As for all the phonon spectra, it also is similar in both samples, which confirms our observation[10] that type-I and type-II magnetite prepare for the transition, on cooling, in a very similar way.

There is a very small but reproducible peak at 19.8 meV [see the inset of Fig. 4(a)], seen in both samples, but behaving differently on cooling: While it remains small and virtually intact for $x = 0.03$, it rises for stoichiometric magnetite, proving some differences in lattice dynamics for two samples at $T < T_V$. On the other hand, the peak at 24 meV, besides moving to lower energies on heating, remains stronger for $x = 0.03$ than for the stoichiometric sample, suggesting different behaviors of the T_{2g} optic mode at $T > T_V$. Also, there is a very small shift to lower energies of the whole spectrum for $x = 0.03$ as compared to $x = 0$, pointing to slightly softer lattices in this case. Finally, the spectra for both samples move to slightly higher energies on cooling [shown only for $x = 0$ in Fig. 4(a)] possibly due to a change in lattice symmetry.

D. Mechanism of the first- and second-order Verwey transition

Our experimental data provide a piece of convincing argument that vibration spectra of first- and second-order magnetite samples are very similar at all temperature ranges. In other words, the lattice vibration contribution cannot explain the easily observed difference between heat capacities of first- and second-order samples at temperatures below the Verwey transition temperature. As mentioned above, no indication of different behaviors of both magnetite classes above T_V is observed (except the peak at 24 meV mentioned above and the small difference in the time spectra, Fig. 3) and the only other clear factor that differentiates between magnetites of first and second order, besides the break in T_V vs x relation, is the diffuse scattering. This diffuse scattering was observed by neutron studies, but also by anomalous x-ray diffraction,[41] the technique sensitive both to crystal lattice as well as to charge-ordering fluctuations. Since the lattice dynamics is very similar for type-I and type-II materials as shown above, these are charge fluctuations that may be different for both classes of materials below T_V.

Thus, the scenario of the Verwey transition might be as follows:

First, at lowest T, the ground state is some stable charge ordering, with the well-documented charge disproportionation of $0.2e$ and with (001) symmetry, followed by a doubled period of orbital ordering: These kinds of distributions are found, e.g., by resonant x-ray scattering[11] and the recent x-ray diffraction studies[42] (where much more complicated patterns of charge disproportionation at the octahedral sites are found). This charge ordering results from the condensation of a few phonon modes described by the irreducible representations of the cubic phase; here, they play the role of order parameters.[9]

Second, there is an excited charge fluctuating state that likely has a wide gap in the stoichiometric magnetite, which prevents its occupation at low temperatures. Therefore, below the first-order phase transition, the critical diffuse scattering and the increase in heat capacity are strongly suppressed. However, this state is sensitive to any lattice imbalance, caused by some element's (Zn, Ti, and nonstoichiometry) presence. For a certain critical concentration, linked possibly to the sudden change in electron-phonon coupling (that may be induced, e.g., by screening of the Coulomb interactions[43]), the energy of this state gets lower, which enables its fast occupation, even at low temperatures, triggering the change in lattice symmetry to cubic. Indeed, a very basic simulation of this state's thermal occupation, based on the two-level Schottky-like model,[44] enables a rough description of the heat capacity, see Fig. 11. Here, total phononic DOS, consisting of experimental partial Fe DOS and the calculated oxygen DOS, was augmented by the two-level system of equal degeneracy, with ~ 170 K (in units of k_B) level separation, simulating charge fluctuation. In the case of first-order magnetite samples, the thermal fluctuations are too low to trigger the transition since the additional state, the one reflected by the $(8\,0\,\frac{3}{4})$ diffuse peak, is not occupied. Ultimately, for higher temperatures, the entropy part of the high-symmetry cubic phase prevails, and the system undergoes discontinuous phase transformation with a simultaneous decrease in energy of this state and its rapid population.

Above the Verwey transition, in both type-I and type-II materials, the charge-orbital order does not disappear completely, but it persists in the form of short-range order, which is reflected in the diffuse scattering found high above T_V. Recent time-resolved resonant x-ray diffraction studies, using the free-electron laser, demonstrated that the transient phase with the charge-orbital ordering may exist even at very high temperatures.[45]

In conclusion, we have presented the experimental arguments, based on the NIS measurements performed on two magnetite single crystals, stoichiometric and Zn doped, that iron lattice dynamics of magnetite, exhibiting the Verwey transition of first and second orders, is similar in the entire temperature range. In both classes of materials, iron DOS changes at T_V, in particular, at the low-energy range, $E < 25$ meV, which however, cannot explain the apparent difference in heat capacity and diffuse scattering between these two classes of materials. This difference can be rationalized if some excitation to different charge-orbital ordering states is considered, which is possible in materials with continuous Verwey transition and is disabled in magnetite of first order. Our calculated phononic DOS reproduces the main features of experimental iron DOS better when the electron-electron interaction parameter $U = 4$ eV is taken into account.

---

[1] A. Gupta and J. Z. Sun, J. Magn. Magn. Mater. **200**, 24 (1999).

[2] R. Aragón, R. J. Rasmussen, J. P. Shepherd, J. W. Koenitzer, and J. M. Honig, J. Magn. Magn. Mater. **54-57**, 1335 (1986).

[3] Z. Tarnawski, A. Wiecheć, M. Madej, D. Nowak, D. Owoc, G. Król, Z. Kąkol, L. Kolwicz-Chodak, A. Kozłowski, and T. Dawid, Acta Phys. Pol. A **106**, 771 (2004).

[4] J. P. Wright, J. P. Attfield, and P. G. Radaelli, Phys. Rev. B **66**, 214422 (2002).

[5] E. I. Terukov, W. Reichelt, D. Ihle, and H. Oppermann, Phys. Status Solidi B **95**, 491 (1979).

[6] Y. Fujii, G. Shirane, and Y. Yamada, Phys. Rev. B **11**, 2036 (1975).

[7] S. M. Shapiro, M. Iizumi, and G. Shirane, Phys. Rev. B **14**, 200 (1976).

[8] R. Aragón, P. M. Gehring, and S. M. Shapiro, Phys. Rev. Lett. **70**, 1635 (1993).

[9] P. Piekarz, K. Parlinski, and A. M. Oleś, Phys. Rev. Lett. **97**, 156402 (2006); Phys. Rev. B **76**, 165124 (2007).

[10] H. Schwenk, S. Bareiter, C. Hinkel, B. Lüthi, Z. Kakol, A. Koslowski, and J. M. Honig, Eur. Phys. J. B **13**, 491 (2000); Z. Kąkol, A. Kozłowski, M. Bałanda, H. Schwenk, B. Luthi, and J. M. Honig, in *Proceedings of the Eighth International Conference on Ferrites (ICF8), Kyoto and Tokyo Japan, 2000*, edited by M. Abe and Y. Yamazaki (The Japan Society of Powder and Powder Metallurgy, Kyoto, Japan), p. 126.

[11] J. E. Lorenzo, C. Mazzoli, N. Jaouen, C. Detlefs, D. Mannix, S. Grenier, Y. Joly, and C. Marin, Phys. Rev. Lett. **101**, 226401 (2008).

[12] I. Leonov, A. N. Yaresko, V. N. Antonov, M. A. Korotin, and V. I. Anisimov, Phys. Rev. Lett. **93**, 146404 (2004).

[13] H.-T. Jeng, G. Y. Guo, and D. J. Huang, Phys. Rev. Lett. **93**, 156403 (2004).

[14] F. Zhou and G. Ceder, Phys. Rev. B **81**, 205113 (2010).

[15] V. A. M. Brabers, F. Walz, and H. Kronmuller, Phys. Rev. B **58**, 14163 (1998).

[16] P. Piekarz, K. Parlinski, and A. M. Oleś, J. Phys.: Conf. Ser. **92**, 012164 (2007).

[17] A. Kozłowski, Z. Kąkol, D. Kim, R. Zalecki, and J. M. Honig, Phys. Rev. B **54**, 12093 (1996); Z. Anorg. Allg. Chem. **623**, 115 (1997).

[18] Z. Kakol *et al.* (unpublished).

[19] B. Handke, A. Kozłowski, K. Parliński, J. Przewoźnik, T. Ślęzak, A. I. Chumakov, L. Niesen, Z. Kąkol, and J. Korecki, Phys. Rev. B **71**, 144301 (2005).

[20] R. Gupta, A. K. Sood, P. A. Metcalf, and J. M. Honig, Phys. Rev. B **65**, 104430 (2002).

[21] L. V. Gasparov, D. B. Tanner, D. B. Romero, H. Berger, G. Margaritondo, and L. Forró, Phys. Rev. B **62**, 7939 (2000).

[22] E. J. Samuelsen and O. Steinsvoll, Phys. Status Solidi B **61**, 615 (1974).

[23] H. R. Harrison and R. Aragón, Mater. Res. Bull. **13**, 1097 (1978).

[24] R. Aragón, H. R. Harrison, R. H. McCallister, and C. J. Sandberg, J. Cryst. Growth **61**, 221 (1983).

[25] M. Seto, Y. Yoda, S. Kikuta, X. W. Zhang, and M. Ando, Phys. Rev. Lett. **74**, 3828 (1995); W. Sturhahn, T. S. Toellner, E. E. Alp, X. Zhang, M. Ando, Y. Yoda, S. Kikuta, M. Seto, C. W. Kimball, and B. Dabrowski, *ibid.* **74**, 3832 (1995).

[26] R. Rüffer and A. I. Chumakov, Hyperfine. Interact. **97**/**98**, 589 (1996).

[27] A. I. Chumakov and W. Sturhahn, Hyperfine. Interact. **123**/**124**, 781 (1999).

[28] V. G. Kohn, A. I. Chumakov, and R. Rüffer, Phys. Rev. B **58**, 8437 (1998); V. G. Kohn and A. I. Chumakov, Hyperfine Interact. **125**, 205 (2000).

[29] P. E. Blöchl, Phys. Rev. B **50**, 17953 (1994).

[30] G. Kresse and D. Joubert, Phys. Rev. B **59**, 1758 (1999).

[31] G. Kresse and J. Furthmüller, Comput. Mater. Sci. **6**, 15 (1996).

[32] J. P. Perdew, K. Burke, and M. Ernzerhof, Phys. Rev. Lett. **77**, 3865 (1996).

[33] V. I. Anisimov, J. Zaanen, and O. K. Andersen, Phys. Rev. B **44**, 943 (1991).

[34] H. J. Monkhorst and J. D. Pack, Phys. Rev. B **13**, 5188 (1976).

[35] K. Parlinski, Z. Q. Li, and Y. Kawazoe, Phys. Rev. Lett. **78**, 4063 (1997).

[36] K. Parlinski, Software PHONON (Kraków, Poland, 2010).

[37] K. Parlinski, in *Neutrons and Numerical Methods*, edited by M. R. Johnson, G. J. Kearley, and H. G. Büttner, AIP Conf. Proc. No. 479 (AIP, New York, 1999), p. 121.

[38] J. Żukrowski *et al.* (unpublished).

[39] M. Seto, S. Kitao, Y. Kobayashi, R. Haruki, Y. Yoda, T. Mitsui, and T. Ishikawa, Phys. Rev. Lett. **91**, 185505 (2003).

[40] M. Hoesch *et al.* (unpublished).

[41] T. Toyoda, S. Sasaki, and M. Tanaka, Jpn. J. Appl. Phys. **36**, 2247 (1997).

[42] J. Blasco, J. Garcia, and G. Subias, Phys. Rev. B **83**, 104105 (2011).

[43] J. P. Shepherd, J. W. Koenitzer, R. Aragon, J. Spalek, and J. M. Honig, Phys. Rev. B **43**, 8461 (1991).

[44] E. S. R. Gopal, *Specific Heats at Low Temperatures* (Heywood, London, 1966).

[45] N. Pontius, T. Kachel, C. Schusler-Langeheine, W. F. Schlotter, M. Beye, F. Sorgenfrei, C. F. Chang, A. Fohlisch, W. Wurth, P. Metcalf, I. Leonov, A. Yaresko, N. Stojanovic, M. Berglund, N. Guerassimova, S. Dusterer, H. Redlin, and H. A. Durr, Appl. Phys. Lett. **98**, 182504 (2011).